Gold Nanoparticle/Polymer Interfaces: All Atom Structures from Molecular Dynamics Simulations

G. Milano,[†,‡,*] G. Santangelo,[§] F. Ragone,[†] L. Cavallo,[†] and A. Di Matteo[§]

[†]Dipartimento di Chimica e Biologia and Research Centre NANO_MATES, Università di Salerno, I-84084, Via Ponte Don Melillo, Fisciano (SA), Italy

[‡]IMAST Scarl-Technological District in Polymer and Composite Engineering, P.le Fermi 1, 80055 Portici (NA), Italy

[§]STMicroelectronics, Via Remo de Feo 1, I-80022 Arzano (NA), Italy

S *Supporting Information*

ABSTRACT: Molecular dynamics simulations have been performed to obtain detailed all-atom models of the interface between polystyrene (PS) and gold nanoparticles. Considering their relevance in the memory technology, systems containing gold nanoparticle included in PS polymer melts also in the presence of 8-hydroxyquinoline (8-HQ) molecules have been studied. Four different systems, including a coated or a non-coated nanoparticle, have been compared. Calculated radial density profiles show that the presence of noncoated nanoparticles in a polymer melt causes an ordering of polymer chains.

ALL ATOM MODELS OF NANOPARTICLE/POLYMER INTERFACES

Coarse-Grained Model

Atomistic Model

A similar ordering behavior is found for the 8-HQ molecule. In the presence of a coated gold nanoparticle, calculated radial density profiles show much less order. When 8-HQ is present, this molecule is closer to the nanoparticle surface and when in contact with a coated nanoparticle it shows a partial penetration into the thiols layer. The molecular description obtained from simulations supports some of the hypothesis made on the basis of the experimental behavior of nonvolatile memory devices.
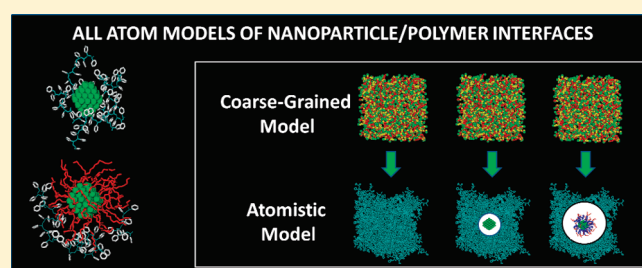
INTRODUCTION

Polymer nanocomposites based on nanometer-sized metal particles are experiencing an explosive growth during the last years due to their technological applications.[1] Organizing inorganic nanoparticles by using soft materials as a matrix is crucial for developing materials with new functionalities.[2] A vast array of applications of this class of materials are emerging in the field of nanoelectronics and have aroused considerable interest because of the unique advantages provided. These advantages include low fabrication cost, high mechanical flexibility, and versatility of the chemical structure. Electronic memories using organic materials such as polymers are industrial targets for the next few years.[3,4]

Memories based on polymeric materials have been achieved by several researchers.[2,5,6] The advantages of this approach are many, the materials used are readily available and easily controlled, the device can be fabricated through simple solution processing, the response time is short, and the operating voltages are low. Furthermore, polymer memories exhibit simplicity in structure, good scalability, low-cost potential, 3D tacking capability, and large capacity for data storage. Advances in memory technology is involving the development of such kinds of nanoscale devices. Bistable molecules,[7,8] donor—acceptor charge transfer complexes,[9,10] and nanocomposites constructed by organic molecules and nanoparticles[2,3,11] are the typical ingredients for the obtainment of these peculiar memory device architectures.

With the development of easy synthetic routes,[12] gold nanoparticles coated with surface thiol layers are used extensively as

building blocks to construct such mesoscopic structures. Yang Yang and co-workers developed several devices based on nanoparticles included into organic or polymeric materials.[13] In particular, organic nonvolatile memory devices made from a polystyrene (PS) film containing gold nanoparticles and 8-hydroxyquinoline (8-HQ) sandwiched between two metal electrodes shows electrical bistability.[2]

The main feature of these devices is a programmable electrical bistability. In particular, at low applied voltage (around 1.0 V) the system shows a low current. The device shows a sharp increase of the current (more than 4 order of magnitudes, from 10^{-11} to 10^{-6} A) if the applied voltage is larger than 2.8 V. After this transition, the device remains in this high-current state even after turning off the power. The high-conductivity state can be erased by applying a negative bias. Several experimental evidence (Discussion section) suggest that an electron transfer occurring between 8-HQ molecules and gold nanoparticles could explain the behavior of this kind of devices. For this reason, a characterization at molecular level of the interfaces between the gold nanoparticles, the polymeric matrix and the 8-HQ molecules could help to understand the behavior of this class of devices and could confirm the hypothesis made on the basis of the electrical behavior. More in general, understanding (and possibly manipulating) the

structure of the interfaces in this new class of materials is fundamental to improve device function and efficiency and would be the key to a bottom-up development of nanoscale devices.

Classical experimental methods for solving the atomic structure of bulk crystals fail for such materials for the intrinsic difficulty to determine atomic arrangements in nanostructured materials. The need to determine atomic arrangements in nanostructured materials has been called the "nanostructure problem",[14] and a procedure to obtain thiol monolayer—protected gold nanoparticle sufficiently uniform in size for the growth of large single crystals for X-ray structure determination has been reported only in the last years.[15] Even more recently, a sophisticated electron microscopy approach coupled with imaging simulation has been proposed as a technique to provide structural insights into gold nanoclusters.[16] Experimental structural information at the atomic level for nanoparticles dispersed in polymer matrices nowadays is extremely difficult especially for the characterization of the interfaces between the nanoparticle and the dispersing polymer phase.

Within the last 10 years, computer simulations have become a predictive tool for addressing structural investigations of complex materials based on polymers.[17−19] However, in the case of nanostructured materials, the computational prediction of detailed molecular structures is still difficult. This is particularly true for polymer-based materials because of the very broad range of length and time scales governing the chain molecular motions.[17]

Many simulation studies to model solid nanoparticles embedded in a polymer matrix have been reported. Most of them use particles without atomistic details. Early studies of coarse-grain models of dense polymer melts containing solid spherical nanoparticles have been conducted with Monte Carlo methods (MC) by Vacatello[20] and with molecular dynamics (MD) simulations by Starr and co-workers.[21] Coarse-grain models have been further applied in various MD[22−27] and MC[28−31] studies to explore general effects such as the size of the nanoparticles, the filling density, and the strength of the nanoparticle—polymer interactions. Brown and co-workers reported an atomistic model of a silica nanoparticle embedded into an amorphous phase of a generic linear polymer modeled at the united-atom level.[33] Then they have carried out detailed all-atom MD simulations on a series of polyethylene oxide (PEO) oligomer—silica nanoparticle systems.[34] For a recent review on theory and simulations of polymer nanocomposites, the reader can refer to ref 32.

In the wake of these studies, the scope of this article is to use molecular dynamics simulations to provide all-atom models of the interfaces between gold nanoparticles and a polymer matrix. For the relevance of these systems in organic memory technology, we focused our attention on programmable devices made from PS film containing gold nanoparticles and 8-HQ. Specifically, we consider model systems made of a gold nanoparticle embedded in a melt of 10-mers of atactic polystyrene as a pure phase or in the presence of a third component (8-HQ molecule) and the effect of nanoparticle coating on the structure of the interfaces. In particular, the results of simulations of four systems containing a gold nanoparticle coated with 1-dodecanthiols included in pure polystyrene melt and in the presence of 8-HQ as a third component and noncoated gold nanoparticles included in pure polystyrene melt and in the presence of 8-HQ as a third component are reported and compared.

Simulations Strategy and Initial Configurations Set Up.
Coarse Graining of PS Model and Reverse Mapping. The present subsection introduces quickly the reader to earlier work and
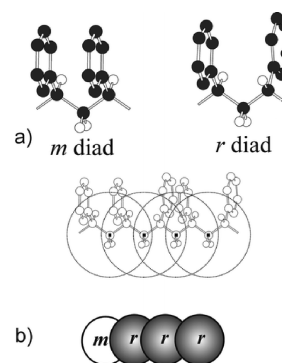
Figure 1. Mapping scheme of the PS adopted coarse-grain model. The atoms belonging to an *m* or *r* diad are grouped in one coarse-grained particle. (a) Atomic structures of *m* and *r* diads. (b) Example of atomistic structure of PS and the corresponding CG model.

concepts that are essential for understanding the present investigation. Further details and extensive validations of the mesoscale approach can be found in refs 35 and 36 and in the Supporting Information.

The basic idea of coarse-grain (CG) models is to group several atoms in one effective bead. This allows us to reach simulation times suitable for the relaxation of polymeric systems reducing the number of degrees of freedom and the computational cost of simulations. The adopted coarse-graining scheme considers a configurational base unit, in particular a diad, as superatom at the mesoscale level. According to this choice, as depicted in Figure 1, the center of a superatom is the methylene carbon.

To have specific CG models, the mesoscale potentials are optimized in a way to reproduce target distributions obtained from reference atomistic simulations. In particular, for intramolecular interaction terms between bonded superatoms (bond and angle potentials) mesoscale potentials obtained by Boltzmann inversion based on a sum of several Gaussian functions have been employed.[37] For the nonbonded part of the potential, pressure-corrected CG numerical potentials optimized by iterative Boltzmann inversion have been used.[38] Further details of the parametrization procedure, including a complete set of distribution plots can be found in refs 35 and 19.

These coarse-grain models have been successfully tested using both MD[35] and, to simulate melts of molar mass up to 210 000 g/mol, by connectivity-altering MC simulations.[19] In both cases, chain dimensions were found in very good agreement with experiments. Furthermore, the equilibrated long-chain configurations reduced to entanglement networks via topological analysis[39] provided a very good estimate of the molar mass between entanglements and of the entanglement tube diameter extracted from plateau modulus measurements. These coarse-grain models have been also used to calculate the viscosity by reverse nonequilibrium molecular dynamics (RNEMD).[40]

In the case of a PS melt, in a series of articles some of us introduced and validated a systematic procedure to obtain well-relaxed all-atom melt structures of polystyrene starting from mesoscale simulations of realistic coarse-grain models.[19,35,36,40] Well relaxed all-atom melts successfully tested against experimental data have been obtained by using a reverse-mapping procedure based on quaternion algebra that, starting from equilibrated mesoscale melt structures, allows a very fast and efficient reconstruction of the atomistic detail. This procedure gives atomistic structures able to reproduce structural experimental

data of large molecular weight stereoregular and stereoirregular PS samples.[36]

Reverse Mapping of Polymer Melt in Presence of a Model Nanoparticle. Here, a similar approach using coarse-grain simulations and successive reverse-mapping has been employed to obtain initial configuration for four different systems modeling a polymer melt including a nanoparticle. In particular, as sketched in part a of Figure 2, as first stage, starting from one configuration obtained by MD equilibration of coarse-grain polymer chains, with periodic boundary conditions, an equilibrated atomistic configuration has been obtained applying the procedure described and validated in ref 36.

The initial configurations of a nanoparticle embedded into a polymer melt have been obtained inserting the gold nanoparticle into a cavity placed in the center of the cubic box. The cavity has been obtained discarding from the back mapping procedure the polymer chains overlapping with the nanoparticle. The chosen overlap criterion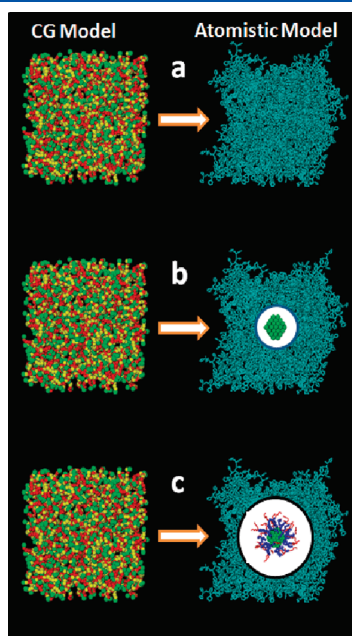 is geometrical. In particular, two atoms are overlapped if the distance between them (scaled by a tolerance coefficient λ chosen between 0.6 and 0.8) was less than the arithmetic average of their Lennard–Jones σ parameters. Further details about this preparatory stage are reported in the Supporting Information.

To avoid possible artifacts depending on the chosen preparation procedures, all systems were subjected to equilibration runs of 6 ns followed by production runs not smaller than 10 ns. Table 1 contains details about all simulated systems.

Simulation Details. All atomistic simulations were performed with the *GROMACS* package.[41] The Berendsen manostat and barostat were used to get a *NPT* ensemble with $\tau_P = 10$ ps and $\tau_T = 0.1$ ps couplings with a time step of 2 fs. All bond lengths were kept constant by the SHAKE algorithm, whereas for non-bonded interactions a cutoff together with a neighbor list of 1.35 nm were used. For CG simulations, the GMQ_num code, a version of the *GMQ* package[42] able to handle numerical potentials and modified to implement multicenterd Gaussian potentials, was used. The simulations were performed at constant temperature (500 K) and constant pressure ($P = 1$ bar) for production runs. The time constants for the loose coupling thermostat and manostat were set to 0.1 and 5 ps. A time step of 15 fs was used. Nonbonded interactions were truncated beyond 15 Å.

The polystyrene all-atom force field employed here has been already used to describe different polystyrene-based materials: polystyrene gels,[43,44] amorphous PS calculation of positronium annihilation spectra,[45] anisotropy of diffusion of helium and CO_2 in a nanoporous crystalline phase of syndiotactic PS.[46] Details about the forcefield and parameters can be found in ref 36.

Both coated and noncoated nanoparticle models are made up of a gold core made of 79 Au atoms organized in a cuboctahedral geometry with a Au–Au bond length of 0.292 nm. The model of coated nanoparticle has 38 thiolate chains. This number has obtained experimentally and reported by Murray et al. for coated nanoparticles of 79 Au atoms in cuboctahedral geometry.[47] Model parameters for gold nanoparticles have been taken from the models of an Au(111) surface coated by alkylthiolate monolayers reported by Ayappa and co-workers.[48] Further details and parameters regarding gold nanoparticles and 8-HQ molecule can be found in the Supporting Information.

■ RESULTS

Polymer Chains and 8-HQ Diffusion. The center of mass mean square displacement (MSD) of PS chains as function of time is shown in Figure 3. From the slope of the curves it is possible to calculate the diffusion coefficients using Einstein's eq 2:

$$6D = \frac{d}{dt}(|R_i(t) - R_i(0)^2|) \qquad (2)$$

where $R_i(t)$ is the position of the ith polymer center of mass at time t. Averaging is performed over all polymer chains as well as

Figure 2. On the left side of a–c, coarse-grain models of polymer melts used for the back mapping procedure are shown. The read beads correspond to m diads the yellow ones to r diads. Coarse-grain particles representing chain end groups are in green. In the atomistic models, the hydrogen atoms are not depicted for clarity. Schematization of the reverse-mapping procedure for the obtainment of initial configurations of (a) PS polymer melt; PS polymer melt containing (b) a noncoated nanoparticle (systems 1 and 3 of table 1). (c) a coated nanoparticle (systems 2 and 4 of Table 1). The coated nanoparticle has been depicted with methyl chain end groups and the four subsequent five methylene carbon atoms, for which in the reverse mapping procedure λ is set equal to 0, in red, the remaining atoms of the chains are in blue.

Table 1. Simulated Systems; All Systems Have Been Simulated at Constant Temperature and Pressure (500 K and 1 bar)

system	no. of PS chains	no. of 8-HQ	total no. of atoms	sim. time [ns]	ρ [kg/m^3]	aver. box size [nm]	D_{PS}x10^6 [cm^2/s]	$D_{8\text{-HQ}}$x10^6 [cm^2/s]
1	Au-NP+PS	145	0	24 004	10.5	1057.9	6.42	1.51	
2	Au-DT+PS	127	0	22 478	13.6	1051.3	6.29	1.48	20.5
3	Au-NP+PS+8-HQ	86	277	19 255	30.0	1072.7	6.10	3.25	
4	Au-DT+PS+8-HQ	86	277	20 699	30.0	1051.6	6.25	3.40	20.8

over time origins. As reported in Table 1, the diffusion coefficients of the polymer chains have similar values, ca. 1.5×10^{-6} cm^2/s, in systems containing noncoated and a coated NP. This value is lower than that calculated at the same temperature for a pure PS melt, 2.4×10^{-6} cm^2/s.[35] This indicates that the presence of a NP in a polymer melt reduces chain mobility. From Figure 3, it is also clear that both curves corresponding to systems including the 8-HQ molecules (systems 3 and 4) show a similar behavior and a higher slope with respect to systems 1 and 2 in which there is a pure polymer phase. This is reasonable because the presence of a lower molecular weight compound increases the mobility of a polymeric material. The resulting center of mass diffusion coefficients for PS chains are 3.25×10^{-6} cm^2/s for the system including a non-coated NP and 3.40×10^{-6} cm^2/s for the system containing a coated NP. Finally, for the smaller 8-HQ molecule 1 order of magnitude larger (Table 1) diffusion coefficients than for PS chains are calculated for both systems 2 and 4.

Radial Density Profiles. The radial mass densities $\rho(r)$ as function of the distance r from the nanoparticle center of mass are shown in Figure 4.

The $\rho(r)$ of part A of Figure 4, corresponding to the radial mass density of PS chains for system 1, containing a noncoated gold nanoparticle in polystyrene as a pure phase, shows two distinct peaks at about 1.3 and 2.3 nm. The first and stronger peak indicates a chain ordering in the vicinity of the nanoparticle. Beyond 2.5 nm the value of the density becomes equal to the polymer melt density. This means that at distances larger than 2.5 nm there is no co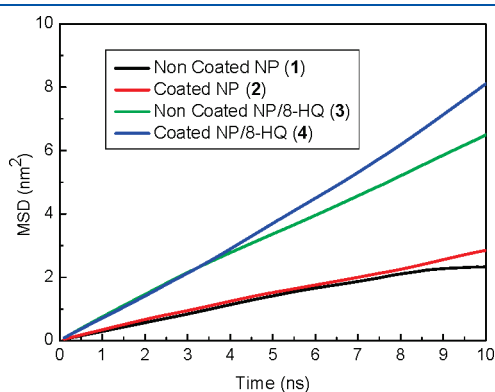rrelation between the presence of the nanoparticle and polymer chain positions. The calculated radius of gyration of the noncoated nanoparticle is 0.53 nm, whereas for a polymer chain is about 0.6 nm. Consistently with previous studies,[20,22,23,28,29,33,34,49] the polymer chains closer to the nano-particle are arranged in two layers. The first one more tightly packed (with a density 60% higher than the melt value), the second one less tightly packed, but still with a density higher (around 6%) than the pure PS melt. The $\rho(r)$ of parat B of Figure 4 shows the behavior of the system in the presence of 8-HQ. The radial density retains the main features of the distribution calculated for a polymer pure phase (part A of Figure 4). A packing of polymer chains close to the nanoparticle is still observed, although in this case a single and weaker peak at 1.3 nm is obtained. As for third component, the first peak (red curve of part B of Figure 4) lies at 1.1 nm indicating some preference for the 8-HQ molecules to be placed at the polymer/ nanoparticle interface.

Differently, a smoother behavior of $\rho(r)$, indicative of less structural organization of the polymer chains, is obtained in the presence of a coated nanoparticle, as seen in Figure 5. Besides a shift of the first peak at larger distances, due to the alkanthiol chains excluded volume interactions (in this case the sum of the nanoparticle 0.89 nm and polymer gyration radius is about 1.5 nm), this system is characterized by a density slowly growing to the maximum value of 1100 kg/m^3 at about 2.2 nm. Similarly, the $\rho(r)$ profile of the 8-HQ (red curve of part B of Figure 5) shows no peaks in the vicinity of the coated nanoparticle. Interestingly, the $\rho(r)$ of 8-HQ shows quite high values (com-parable with the value at long distances) already for distances smaller than the nanoparticle radius of gyration. This indicates some penetration of the 8-QH molecules inside the dode-canthiols layer. This feature will be more clear and will be treated in a more detailed way in the following where the atomic contributions to the radial density will be discussed.

The atomic radial mass densities $\rho(r)$ as function of the distance r from the nanoparticle center of mass are shown in Figure 6, where the density due to the backbone to the phenyl rings and to the end groups carbon atoms of the polymer chains have been reported separately. Focusing on the system contain-ing a noncoated nanoparticle in a pure polymer phase, part A of Figure 6, it is worth noting that the phenyl rings are closer to the nanoparticle/polymer interface (red curve of part A of Figure 6), with nonzero values of the density starting from 0.6 nm. The polymer chain end groups radial density, as seen in part B of Figure 6, clearly indicates a slightly higher concen-tration of end groups at a distance of about 1 nm from the nanoparticle center of mass.

Figure 3. Mean square displacements vs time calculated for the center of mass of PS chains in the four considered systems. The two curves corresponding to systems 3 and 4 containing 8-HQ molecules show largers slopes with respect to the systems with a pure polymer phase.
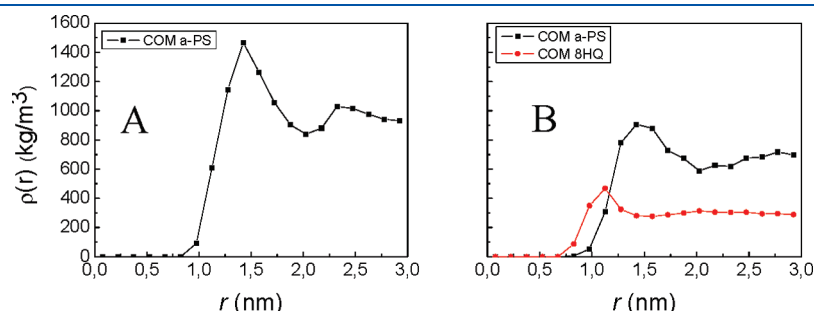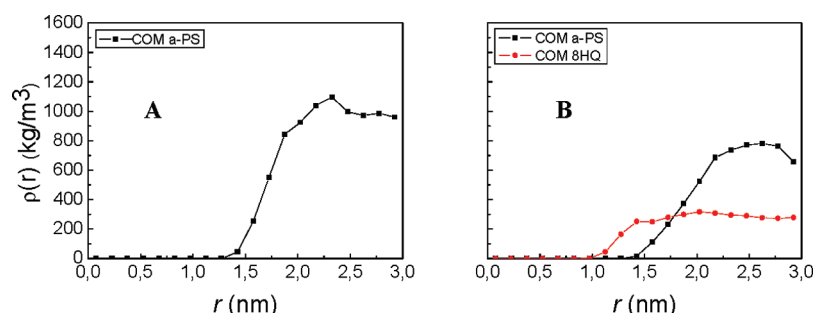

Figure 4. Radial density profiles of the center of mass of PS chains for systems containing a noncoated gold nanoparticle as function of the distance from NP center of mass. (A) System 1. (B). System 3. In red is reported the calculated radial density for the center of mass of 8-HQ molecules.

Figure 5. Radial density profiles of the center of mass of PS chains, for systems containing coated gold nanoparticle. nanoparticle as function of the distance from NP center of mass. (A) System 2. (B). System 4. In red is reported the calculated radial density for the center of mass of 8-HQ molecules.
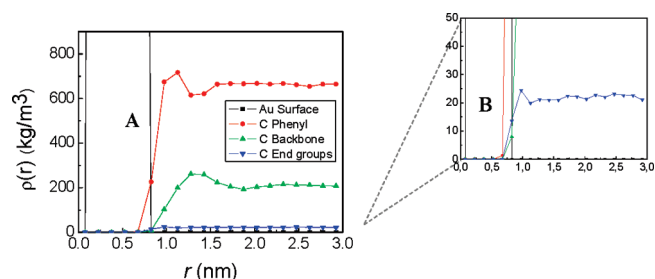

Figure 6. Atomic radial mass densities as function of the distance from the NP center of mass for system containing a noncoated nanoparticle in a pure polymer phase.
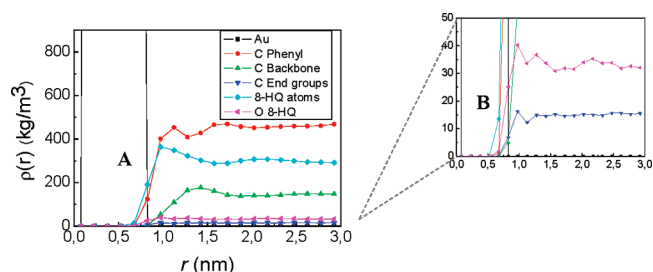

Figure 8. Atomic radial mass density as function of the distance from the NP center of mass for system containing a noncoated nanoparticle in a polymer phase in the presence of 8-HQ molecules.
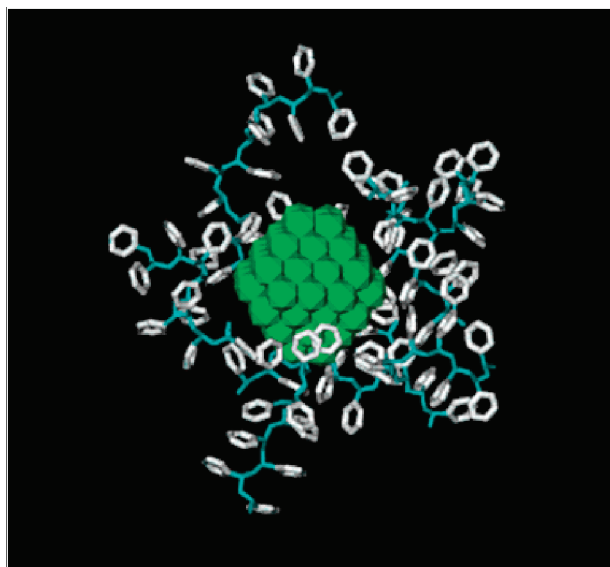

Figure 7. Snapshot of system 1, showing some polymer chains closer to the nanoparticle surface. Polymer chains approach the nanoparticle surface exposing mainly the phenyl rings (white color). The backbone carbons are in blue, hydrogen atoms are omitted for clarity.

Figure 9. Atomic radial mass densities as function of the distance from the NP center of mass for the system 2 containing a coated nanoparticle in a pure polymer phase.

A typical configuration of the polymer chains close to the nanoparticle is shown in Figure 7, and it is clear that the polymer chains approach the nanoparticle surface exposing mainly phenyl rings.

The $\rho(r)$ for the system containing a noncoated nanoparticle in polymer phase in the presence of 8-HQ is shown in Figure 8. Similarly to the pure polymer system, the phenyl carbon atoms are closer to the nanoparticle but the peak is less pronounced
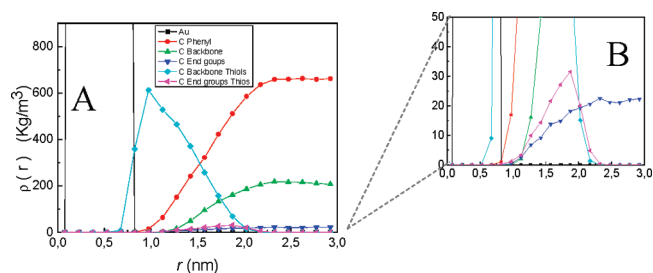
showing less structuring of the polymer around the nanoparticle (this different behavior is also apparent in the center of mass radial densities). In this case also the atoms of 8-HQ are close to the nanoparticle surface. Nonzero values of radial density of atoms of 8-HQ start from about 0.6 nm. Also, in this case there is a higher concentration of the polymer end groups at a distance of about 1 nm from the nanoparticle center of mass, as seen in part B of Figure 8.

The $\rho(r)$ for the system containing a coated nanoparticle in a pure polymer phase is reported in Figure 9. The alkanthiolate carbon chains density (aqua curve of part A of Figure 9) shows nonzero values until 2.0 nm. This length can be considered as the maximum average nanoparticle radius. Also, in this case the atoms closer to the interface are the phenyl ring carbons. Is worth noting that the curves of the radial density of alkanthiol carbons and the one related to polymer chains largely overlap in the region going from 0.7 to 2 nm from the NP center of mass. This indicates that the polymer chains atoms, especially the one of phenyl rings, penetrate, to some extent, inside the alkanthiolate chains layer. In fact, nonzero values of the radial densities of
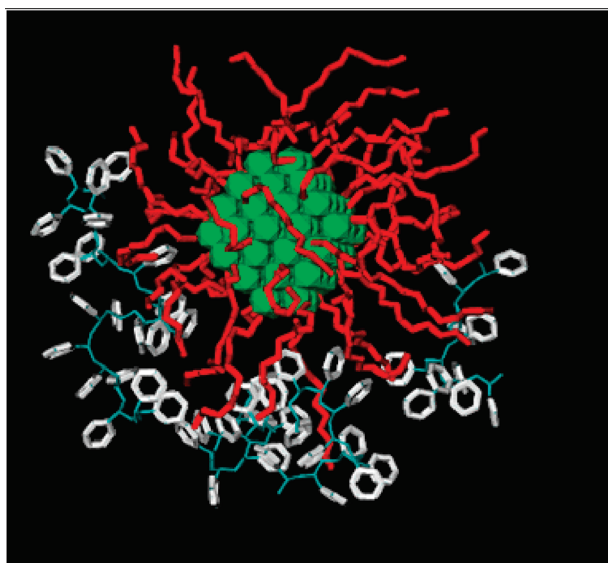
Figure 10. Snapshot of system 2, showing some polymer chains closer to the nanoparticle surface. Similarly, to system 1 (shown in Figure 7), polymer chains approach the nanoparticle surface exposing mainly the phenyl rings (white color) some of the phenyl rings penetrate trough the alkyl chains layer (in red). The backbone carbons are in blue, the thiols chaons are depicted in red, hydrogen atoms are omitted for clarity.

Figure 11. Atomic radial mass densities as function of the distance from the NP center of mass for the system 2 containing a coated nanoparticle in a polymer phase in the presence of 8-HQ molecules.

phenyl carbon atoms can be observed starting from 0.7 nm. In contrast with the behavior of the system including a noncoated nanoparticle, the radial density of carbon atoms of both phenyl rings and backbone grows more smoothly and without showing a maximum.

Differently from the behavior of the systems with a noncoated nanoparticle, no higher concentration of polymer chain end groups close to the gold surface neither in the region of alkathiolate chains is observed. In particular, the density reported in part B of Figure 9 clearly indicates that the polymer chain end group radial density increases smoothly from zero starting from about 1 nm from the nanoparticle center of mass and reaches the bulk value at 2.1 nm from the nanoparticle center of mass. The radial density of thiolate alkyl chains end groups shows a maximum around 2 nm, which is in the region of the nanoparticle polymer interface. A typical configuration of the system, showing the polymer chains close to the coated nanoparticle, is reported in Figure 10, where it is clear that the polymer chains approach the nanoparticle surface exposing the phenyl rings (white atoms), whereas some of the rings penetrate through the alkyl chains (in red) layer.

The radial densities of the system including a coated nanoparticle in a polymer phase in the presence of 8-HQ are shown in part A of Figure 11. Similarly to the pure polymer system, the phenyl carbon atoms are close to the nanoparticle, and the overlap between the curves related to phenyl and backbone carbon atoms and to the alkyl chains of the nanoparticle indicates that some penetration of the polymer chains inside the coating layer is observed also in this case. However, here the atoms closer to the gold surface are the 8-HQ ones. In fact, the curve related to the 8-HQ atoms radial density starts to show nonzero value from about 0.6 nm and finally grows to bulk values starting from distances from the nanoparticle center of mass of about 2 nm.

Is worth noting that, in the case of the noncoated nanoparticle, the 8-HQ molecules are close to the nanoparticle surface together with the carbon atoms of the phenyl groups (the two
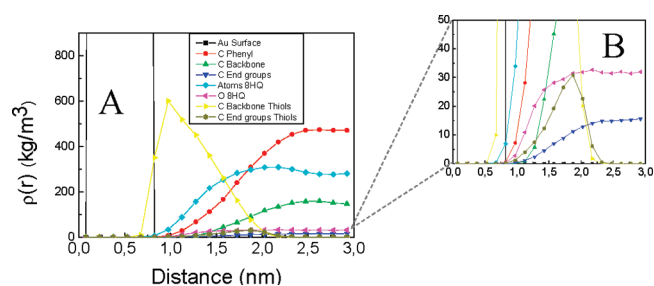
curves of Figure 8 corresponding to 8-HQ and phenyl carbon overlap in the region close to the gold surface). In contrast, in the case of the coated NP, shown in part A of Figure 11, the radial density of 8-HQ atoms results closer to the NP center of mass and the curve corresponding to the phenyl ring is shifted at a larger distance. Furthermore, in the case of part A of Figure 11, the radial density of 8-HQ atoms grows more smoothly than the one shown in Figure 8 and does not show peaks. Also, in this case the radial density of NP alkyl chains end groups shows a maximum at around 2 nm in the region of the nanoparticle polymer interface.

Polymer Chain Dimension. The behavior of end-to-end distance and radius of gyration of the PS chains as a function of the distance between the nanoparticle and chain center of mass are reported in Figure 12. In the case of systems including a noncoated nanoparticle, as seen in part A of Figure 12, it is clear that for both pure polymer phase and in the presence of 8-HQ there is an increase of the dimension for the chains closer to the nanoparticle. At a short distance from the nanoparticle, there is an increase of about 6% (black curve in part A of Figure 12) in the end-to-end distance from the value of the melt. For the system including 8-HQ (red curve in part A of Figure 12), there is a similar increase, about 7%, of the chain dimension. At distances larger than 2 nm, the chain dimension converges to the value of the pure PS melt. The results are similar for the system including 8-HQ (red curve of part A of Figure 12). For the systems, the behavior of the radius of gyration shows trends similar to the end-to-end distance. Rather similar is the behavior in the presence a coated nanoparticle, as seen in part B of Figure 12, with an increase of the chain dimension close to the nanoparticle, whereas at a larger distance the chain dimension converges to the value of the pure polymer melt. The system in the pure polymer phase shows a chain expansion of about 8% with respect to the value of the pure polymer melt close to the nanoparticle. In the presence of 8-HQ (red curve of part B of Figure 12), the chain expansion is about 5%.

Both for noncoated and for coated nanoparticles in the case of pure polymer phase as well as in the presence of 8-HQ, an increase of the chain dimension going from 5 to 8% is found. A similar behavior has been obtained in simulations of bead and spring chains in contact with a nanoparticle by Glotzer et al.,[25] and the increase in the dimension was found to be of the order of 20%. Brown and co-workers found an expansion of the polymer chain dimension of the order of 15% in the case of molecular dynamics simulations of PEO oligomers in contact with a silica nanoparticle.[34] The smaller expansion values that we obtained are probably due to the larger stiffness of PS with respect to more flexible bead and spring models and atomistic PEO chains.

Orientation of 8-HQ Molecules. The orientation of 8-HQ with respect to the nanoparticle can be characterized using molecule-fixed unit vectors. The structures of the gold nanoparticle and 8-HQ together with the vectors used to characterize the orientation of 8-HQ with respect the 111 surface of the nanoparticle are schematized in Figure 13, where the vectors $\hat{u}_{NP}$ perpendicular to the eight 111 surfaces of the octahedral nananoparticle and the three vectors $\hat{u}_1$, $\hat{u}_2$, and $\hat{u}_3$ are depicted. We arbitrarily take as unit vector $\hat{u}_1$ the in-plane vector along the bond shared by the two rings of 8-HQ. The other in-plane vector $\hat{u}_2$ is perpendicular to $\hat{u}_1$ and joins the middle of the two C—C bonds parallel to the central C—C bond. A third orientation vector $\hat{u}_3$ obtained by the vector product of $\hat{u}_1, \times \hat{u}_2$ is normal to the molecular plane.

The orientation of the 8-HQ molecule with respect to the nanoparticle, as function of the distance between the nanoparticle and 8-HQ center of mass, has been characterized calculating a suitable orientation function averaged over different molecules, for all eight $\hat{u}_{NP}$ vectors and simulation time. In particular, the

mutual orientation of the nanoparticle surface and the 8-HQ molecular plane can be obtained considering the angle between the vectors $\hat{u}_{NP}$ (perpendicular to the 111 nanoparticle surface) and $\hat{u}_3$ perpendicular to the molecular plane of 8-HQ. The averaged order parameter P_2 of the angle between the vectors $\hat{u}_{NP}$ and $\hat{u}_3$ as function of the distance for the system containing a noncoated nanoparticle in the presence of 8-HQ is reported in Figure 14.

The order parameter P_2 has been obtained calculating the second order Legendre polynomial $P_2 = 1/2\langle 3\cos^2\theta - 1\rangle$. Values of P_2 close to one indicate a predominance of parallel or antiparallel orientation of two vectors, values close to -0.5 indicate a predominance of perpendicular orientation. Random orientations give values of P_2 equal to zero.

According to the definitions given above, the curves reported in Figure 14 clearly indicate that for distances between the nanoparticle and 8-HQ center of mass lower than 1.2 nm the 8-HQ molecules are oriented with the molecular plane parallel to the nanoparticle surface. The radial density of 8-HQ molecules, also reported in Figure 14, clearly indicates that, at short distances,
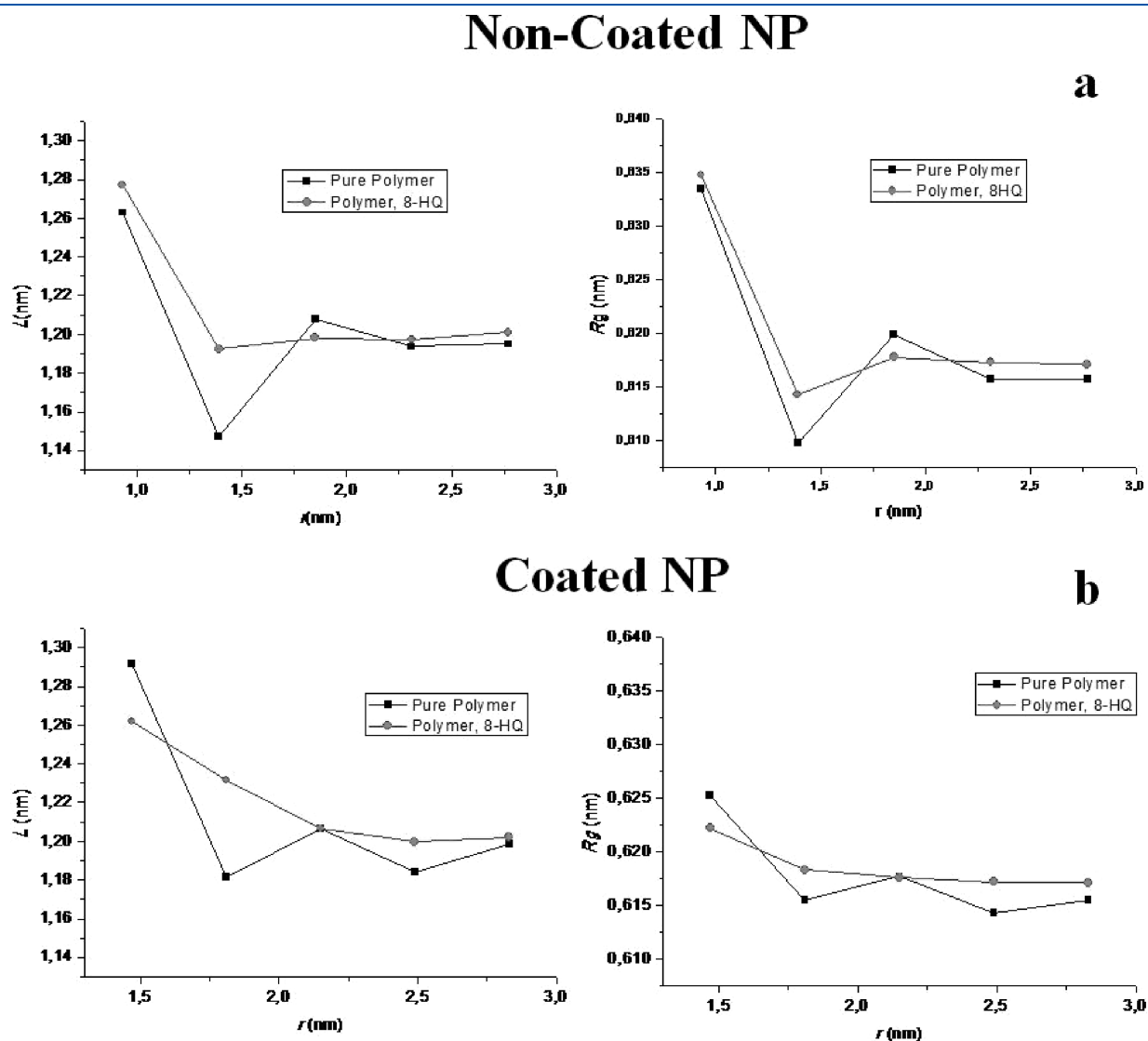

Figure 12. (a) PS end-to-end distance (L) and radius of gyration (R_g) as function of distance between NP and PS center of mass for systems 1 (black curves) and 3 (red curves) containing a noncoated nanoparticle. (b) PS end-to-end distance (L) and radius of gyration (R_g) as function of distance between NP and PS center of mass for systems 2 (black curves) and 4 (red curves) containing a coated nanoparticle.
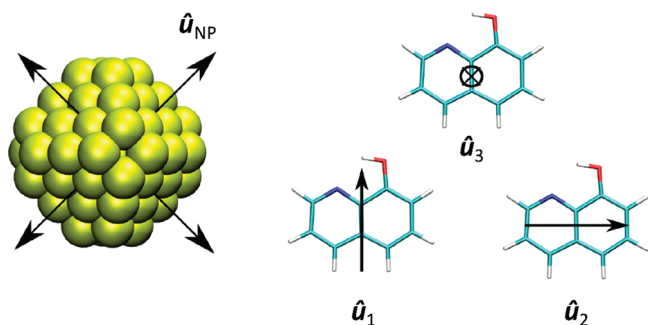
Figure 13. Schematized structures of gold nanoparticle and 8-HQ together with the vectors used to characterize the orientation of 8-HQ with respect the nanoparticle 111 surface. Four among eight possible $\hat{u}_{NP}$ vectors perpendicular to the nanoparticle surfaces are shown is the figure.
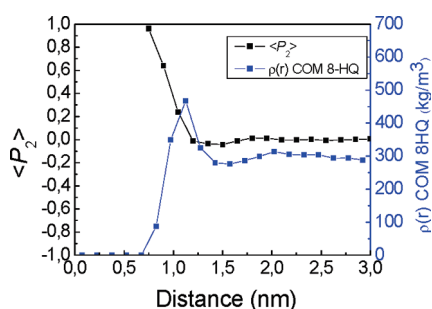

Figure 14. P_2 order parameter of the angle between the vectors $\hat{u}_{NP}$ and $\hat{u}_3$ (Figure 13) as function of the distance between NP and 8-HQ centers of mass for the system containing a noncoated nanoparticle in the presence of 8-HQ. The blue curve shows the behavior of 8-HQ center of mass radial density.

Figure 15. Snapshot of system 3, showing three 8-HQ molecules close to the nanoparticle surface. According to the analysis of orientation functions shown in Figure 13, the 8-HQ molecules orient the molecular plane parallel to the NP surface.

Figure 16. P_2 order parameter of the angle between the vectors $\hat{u}_{NP}$ and $\hat{u}_3$ (Figure 13) as function of the distance between NP and 8-HQ centers of mass for the system containing a coated nanoparticle in the presence of 8-HQ. The red curve shows the behavior of thiols carbon atoms density. The blue curve shows the behavior of 8-HQ center of mass radial density.

where the orientation is stronger, the radial density is low. The nanoparticle radius is about 0.6 nm and this means that when the distance between 8-HQ and nanoparticle center of mass is about 0.6 nm the molecules are attached to the surface. According to this, the few molecules 8-HQ that are very close to the surface have a strong parallel orientation. This behavior is reasonable due to the excluded volume interactions between atoms of the gold surface and the atoms of the 8-HQ molecules. At distances where the radial density is larger (~1 nm) the parallel orientation is still present but less prevalent. Finally, at distances larger than 1.2 nm the plot of Figure 14 indicates a random orientation.

A snapshot of the simulated systems including a noncoated nanoparticle, depicted in Figure 15, clearly shows some of the 8-HQ molecules closer to the gold surface, and in a nearly parallel orientation to the nanopartcile surface.

The averaged order parameter P_2 of the angle between the vectors $\hat{u}_{NP}$ and $\hat{u}_3$ as function of the distance for the system containing a coated nanoparticle in the presence of 8-HQ is reported in Figure 16.

At very short distances, between 0.6 and 0.7 nm from the nanoparticle center of mass, the molecular plane is oriented parallel to the nanoparticle surface. In this case, as it is possible to see from the plot of the 8-HQ radial density, the radial density is practically zero. The region from 1.0 to about 1.5 nm away from the center of mass corresponds to higher density of alkyl chains (i.e., the nanoparticle corona). In this region, as already noted in the previous section, the density of 8-HQ is relevant. The
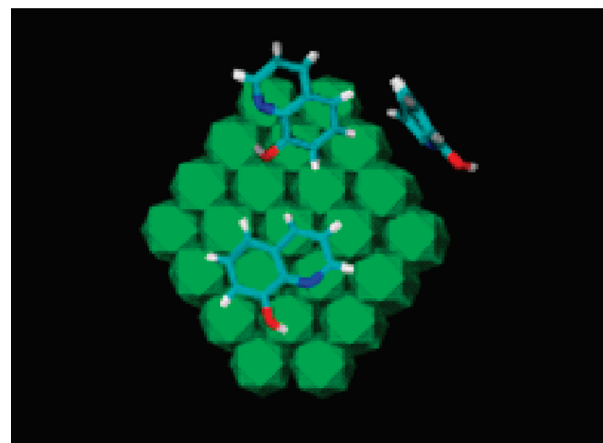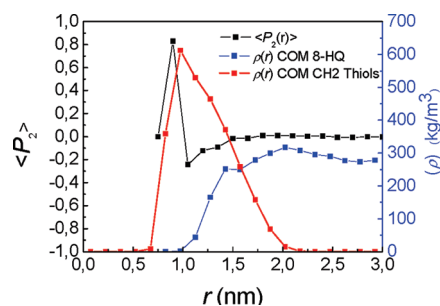
behavior of the average P_2 in this region is characterized by negative values ranging from −0.3 to 0 at distances larger than 1.5 nm. This indicates a preference for the 8-HQ molecules penetrating inside the region with high density of alkyl chains to orient perpendicular to the gold surface. A snapshot of the simulation of the system including a coated nanoparticle in the presence of 8-HQ, depicted in Figure 17, clearly shows the penetration of the 8-HQ molecules through the coating layer and their tendency to be perpendicular to the gold surfaces.

■ DISCUSSION

In this section, we try to use insights from the simulations to understand the behavior of electronic devices based on coated gold NP dispersed in PS reported in ref 2. On the basis of the macroscopic electrical behavior of the electronic devices, several hypothesis on the molecular mechanism underlying the switching process and the different role of the molecular constituents have been formulated by Yang and co-workers. In particular, two main experimental evidence obtained by Yang and co-workers (fast transitions on the nanosecond scale and a temperature independent process) suggested tunneling, that is an electron transfer between 8-HQ molecules and the coated gold
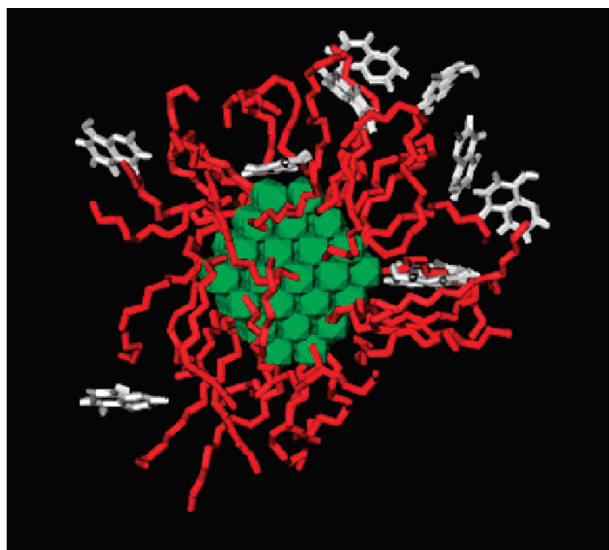
Figure 17. Snapshot of system 4, showing some 8-HQ molecules close to the coating layer. According to the analysis of orientation functions shown in Figure 16, the 8-HQ molecules have the tendency to orient the molecular plane l to the NP surface.

nanoparticles, as the mechanism underlying the device switching process. According to the proposed mechanism, the coating layer should play a crucial role. The stability of the state having an electron localized on the gold nanoparticle can be ascribed to the insulation of the coating layer, which should prevent the electron transfer back to 8-HQ molecules when the electric field is switched off. As regards PS, ac-impedance studies show that PS acts as an inert matrix for coated nanoparticles and 8-HQ, and should not play a part in the electronic transition. With this background in mind, our simulations allow to affirm that:

a) the presence of the coating layer on the gold nanoparticles shifts the 8-HQ molecules away from the NP surface and reduces a structuring of these molecules;

b) the behavior of the polymer chains is influenced by the presence of coating. Also, in this case the strong structuring close to the metal surface, typical of noncoated nanoparticles, is absent when the nanoparticle is coated;

c) the molecular orientation is also affected by the presence of the coating layer. In particular, the 8-HQ that are closer to the nanoparticle are oriented with the molecular plane perpendicular to the NP surface.

The molecular picture resulting from the simulations can confirm some of the hypothesis made on the basis of macroscopic device behavior. In particular, the insulating effect of the coating layer is supported by results of point a. Another relevant effect of the coating layer is the cancellation of the structuring of PS chains around the nanoparticle (point b). This feature supports the hypothesis that the polymer matrix is practically inert. Finally, information about 8-HQ molecular orientation summarized as point c can be useful as a starting point for further computational studies aimed at understanding the mechanism of electron transfer by using quantum mechanical computational methods.

CONCLUSIONS

Using MD simulations, interfaces between gold nanoparticle and PS melts have been characterized at the atomic level.

Considering their relevance in memory technology applications, systems containing gold nanoparticle included in PS polymer melts also in the presence of 8-HQ molecules have been studied.

Four different systems have been compared. To understand the effect of nanoparticle coating on the interfaces structure, results obtained for systems including coated and noncoated gold nanoparticles in a PS melt have been compared. Furthermore, the effects of the presence of a third low molecular weight component (8-HQ) and its orientation with respect to noncoated and coated gold nanoparticles have been considered.

In agreement with previous studies, the calculated radial density profiles show that the presence of noncoated nanoparticles in a polymer melt causes an ordering of the polymer chains. This effect is less pronounced but still present for PS chains in the presence of the lower molecular weight 8-HQ third component. A similar ordering behavior is found for the 8-HQ molecule.

In presence of a coated gold nanoparticle, the calculated radial density profiles show much less order for both PS chains and 8-HQ molecules with respect to systems including a noncoated nanoparticle.

Atomic contributions to the radial density profiles reveal that, both for noncoated and coated gold nanoparticles, PS chains expose the phenyl rings to the nanoparticle surface. In the case of coated nanoparticles, there is some penetration of the PS phenyl rings into the nanoparticle coating layer. When 8-HQ is present, this molecule is closer to the nanoparticle surface and when in contact with a coated nanoparticle partially penetrates into the thiols layer.

In the case of noncoated gold nanoparticles, the orientation of 8-HQ is short ranged and parallel with respect to the surface of the nanoparticle. Differently, in the case of a coated gold nanoparticle the 8-HQ molecule assumes an orientation nearly perpendicular to the nanoparticle surface.

In conclusion, the molecular description obtained from simulations results supports some of the hypothesis made on the basis of macroscopic device behavior.

ASSOCIATED CONTENT

S **Supporting Information.** This material is available free of charge via the Internet at http://pubs.acs.org.

AUTHOR INFORMATION

Corresponding Author
*Phone: +39-089-969567; fax:+39-089-969602; e-mail: gmilano@unisa.it.

REFERENCES

(1) Koo, J. H. *Polymer Nanocomposites*; Mcgraw-Hill: New York, 2006.
(2) Ouyang, J. Y.; Chu, C. W.; Szmanda, C. R.; Ma, L. P.; Yang, Y. *Nat. Mater.* **2004**, 3, 918.

(3) Lee, S. W.; Mao, C. B.; Flynn, C. E.; Belcher, A. M. *Science* **2002**, *296*, 892.

(4) Bozano, L. D.; Kean, B. W.; Deline, V. R.; Salem, J. R.; Scott, J. C. *Appl. Phys. Lett.* **2004**, *84*, 607.

(5) Moller, S.; Perlov, C.; Jackson, W.; Taussig, C.; Forrest, S. R. *Nature* **2003**, *426*, 166.

(6) Tseng, R. J.; Baker, C. O.; Shedd, B.; Huang, J. X.; Kaner, R. B.; Ouyang, J. Y.; Yang, Y. *Appl. Phys. Lett.* **2007**, *90*.

(7) Collier, C. P.; Wong, E. W.; Belohradsky, M.; Raymo, F. M.; Stoddart, J. F.; Kuekes, P. J.; Williams, R. S.; Heath, J. R. *Science* **1999**, *285*, 391.

(8) Cai, L. T.; Cabassi, M. A.; Yoon, H.; Cabarcos, O. M.; McGuiness, C. L.; Flatt, A. K.; Allara, D. L.; Tour, J. M.; Mayer, T. S. *Nano Lett.* **2005**, *5*, 2365.

(9) Chu, C. W.; Ouyang, J.; Tseng, H. H.; Yang, Y. *Adv. Mater.* **2005**, *17*, 1440.

(10) Ling, Q. D.; Song, Y.; Ding, S. J.; Zhu, C. X.; Chan, D. S. H.; Kwong, D. L.; Kang, E. T.; Neoh, K. G. *Adv. Mater.* **2005**, *17*, 455.

(11) Tseng, R. J.; Huang, J. X.; Ouyang, J.; Kaner, R. B.; Yang, Y. *Nano Lett.* **2005**, *5*, 1077.

(12) Daniel, M. C.; Astruc, D. *Chem. Rev.* **2004**, *104*, 293.

(13) Yang, Y.; Ouyang, J.; Ma, L.; Tseng, R. H.; Chu, C. W. *Adv. Funct. Mater.* **2006**, *16*, 1001.

(14) Billinge, S. J. L.; Levin, I. *Science* **2007**, *316*, 561.

(15) Jadzinsky, P. D.; Calero, G.; Ackerson, C. J.; Bushnell, D. A.; Kornberg, R. D. *Science* **2007**, *318*, 430.

(16) Li, Z. Y.; Young, N. P.; Di Vece, M.; Palomba, S.; Palmer, R. E.; Bleloch, A. L.; Curley, B. C.; Johnston, R. L.; Jiang, J.; Yuan, J. *Nature* **2008**, *451*, 46.

(17) Baschnagel, J.; Binder, K.; Doruker, P.; Gusev, A. A.; Hahn, O.; Kremer, K.; Mattice, W. L.; Muller-Plathe, F.; Murat, M.; Paul, W.; Santos, S.; Suter, U. W.; Tries, V. In *Advances In Polymer Science: Viscoelasticity, Atomistic Models, Statistical Chemistry*; **2000**; Vol. *152*, p 41.

(18) Muller-Plathe, F. *ChemPhysChem* **2002**, *3*, 754.

(19) Spyriouni, T.; Tzoumanekas, C.; Theodorou, D.; Muller-Plathe, F.; Milano, G. *Macromolecules* **2007**, *40*, 3876.

(20) Vacatello, M. *Macromolecules* **2001**, *34*, 1946.

(21) Starr, F. W.; Schroder, T. B.; Glotzer, S. C. *Phys. Rev. E* **2001**, *6402*.

(22) Starr, F. W.; Schroder, T. B.; Glotzer, S. C. *Macromolecules* **2002**, *35*, 4481.

(23) Smith, G. D.; Bedrov, D.; Li, L. W.; Byutner, O. *J. Chem. Phys.* **2002**, *117*, 9478.

(24) Desai, T.; Keblinski, P.; Kumar, S. K. *J. Chem. Phys.* **2005**, *122*.

(25) Starr, F. W.; Douglas, J. F.; Glotzer, S. C. *J. Chem. Phys.* **2003**, *119*, 1777.

(26) Kairn, T.; Daivis, P. J.; Ivanov, I.; Bhattacharya, S. N. *J. Chem. Phys.* **2005**, *123*.

(27) Sen, S.; Thomin, J. D.; Kumar, S. K.; Keblinski, P. *Macromolecules* **2007**, *40*, 4059.

(28) Vacatello, M. *Macromolecules* **2002**, *35*, 8191.

(29) Vacatello, M. *Macromolecules* **2003**, *36*, 3411.

(30) Zhang, Q.; Archer, L. A. *J. Chem. Phys.* **2004**, *121*, 10814.

(31) Papakonstantopoulos, G. J.; Yoshimoto, K.; Doxastakis, M.; Nealey, P. F.; de Pablo, J. J. *Phys. Rev. E* **2005**, *72*.

(32) Allegra, G.; Raos, G.; Vacatello, M. *Prog. Polym. Sci.* **2008**, *33*, 683.

(33) Brown, D.; Mele, P.; Marceau, S.; Alberola, N. D. *Macromolecules* **2003**, *36*, 1395.

(34) Barbier, D.; Brown, D.; Grillet, A. C.; Neyertz, S. *Macromolecules* **2004**, *37*, 4695.

(35) Milano, G.; Muller-Plathe, F. *J. Phys. Chem., B* **2005**, *109*, 18609.

(36) Santangelo, G.; Di Matteo, A.; Muller-Plathe, F.; Milano, G. *J. Phys. Chem., B* **2007**, *111*, 2765.

(37) Milano, G.; Goudeau, S.; Müller-Plathe, F. *J. Polym. Sci., Part B: Polymer Physics* **2005**, *43*, 871.

(38) Reith, D.; Pütz, M.; Müller-Plathe, F. *J. Comput. Chem.* **2003**, *24*, 1624.

(39) Tzoumanekas, C.; Theodorou, D. N. *Macromolecules* **2006**, *39*, 4592.

(40) Chen, X. Y.; Carbone, P.; Cavalcanti, W. L.; Milano, G.; Mueller-Plathe, F. *Macromolecules* **2007**, *40*, 8087.

(41) Berendsen, H. J. C.; van der Spoel, D.; van Drunen, R. *Comput. Phys. Commun.* **1995**, *91*, 43.

(42) *gmq User Manual Version 3,* http://www.univ-savoie.fr/labos/lmops/brown/gmq.html; Brown, D., Ed.

(43) Muller-Plathe, F. *Macromolecules* **1996**, *29*, 4782.

(44) Witt, R.; Sturz, L.; Dolle, A.; Muller-Plathe, F. *J. Phys. Chem., A* **2000**, *104*, 5716.

(45) Schmitz, H.; Muller-Plathe, F. *J. Chem. Phys.* **2000**, *112*, 1040.

(46) Milano, G.; Guerra, G.; Müller-Plathe, F. *Chem. Mater.* **2002**, *14*, 2977.

(47) Hostetler, M. J.; Wingate, J. E.; Zhong, C.-J.; Harris, J. E.; Vachet, R. W.; Clark, M. R.; Londono, J. D.; Green, S. J.; Stokes, J. J.; Wignall, G. D.; Glish, G. L.; Porter, M. D.; Evans, N. D.; Murray, R. W. *Langmuir* **1998**, *14*, 17.

(48) Rai, B.; Sathish, P.; Malhotra, C. P.; Pradip; Ayappa, K. G. *Langmuir* **2004**, *20*, 3138.

(49) Borodin, O.; Smith, G. D.; Bandyopadhyaya, R.; Byutner, E. *Macromolecules* **2003**, *36*, 7873.

J

dx.doi.org/10.1021/jp201374h |*J. Phys. Chem. C* XXXX, XXX, 000–000